Special Crystal Growth and Nucleation process of Zinc Oxide Nanoparticles from Urea Solution for Efficient Removal of Pb(II) ions and Alizarin Red S

John Godwin (godwinjohn1380@gmail.com)
Kogi State college of education (technical), kabba, Nigeria.
Nasir Abdus-Salam
University of Ilorin
Prasanna Kumar Panda
Institute of Minerals and Materials Technology
Bankim Chandra Tripathy
Institute of Minerals and Materials Technology

Research Article

Keywords: ZNPs-adsorbent, synthesis/characterization, adsorption, isotherms, kinetics, thermodynamic

Posted Date: May 26th, 2022

DOI: https://doi.org/10.21203/rs.3.rs-1625280/v1

Special Crystal Growth and Nucleation process of Zinc Oxide Nanoparticles from Urea Solution for Efficient Removal of Pb(II) ions and Alizarin Red S

John Godwin.[a,b,c], Nasir Abdus-Salam,[b], Prasanna Kumar Panda[c], and Bankim Chandra Tripathy[c]

[a]Department of Chemistry, Kogi State College of Education (Technical), P.O.B 242 Kabba, Nigeria.
[b]Department of Chemistry, University of Ilorin, P.M.B. 1515, Ilorin, Nigeria
[c]Hydro & Electrometallurgy Department, Institute of Minerals and Materials Technology, Bhubaneswar - 751 013, India

Corresponding author: John Godwin; Department of Chemistry, School of Sciences, Kogi State College of Education (Technical), P.O.B 242 Kabba, Nigeria. Phone number: +2348068675243 e-mail: godwinjohn1380@gmail.com

Abstract

Zinc oxide nanoparticles (ZNPs) were prepared from $Zn(NO_3)_2.6H_2O$ and CON_2H_4. X-ray Diffraction (XRD), Scanning Electron Microscopy (SEM), Energy Dispersion Atomic X-ray (EDAX), Transmission Electron Microscopy (TEM), and Thermogravimetric-Differential Thermal Analysis (TGA/DTA) were utilized for determination of the composition, morphology, elemental analysis, crystallinity, and thermal stability respectively, while Fourier-Transform Infrared Spectroscopy (FTIR) method was used to determine the functional groups present in the ZNPs. The adsorption of Pb(II) and Alizarin Red S (ARS) onto ZNPs were investigated at different solution pH, concentration, adsorbent mass, temperature and contact time. The optimum adsorption capacity of Pb(II) on ZNPs was 341.65 mg/g at pH 10 in 180 minutes at 318 K. Similarly, the optimum adsorption capacity of ARS was found to be 18.84 mg/g at pH 4 in 180 minutes at 318 K. The Langmuir isotherm model fitted well with regression coefficient, $R^2 = 0.9252$ and 0.9035 for Pb(II) and ARS respectively. Th pseudo-second-order kinetics with $R^2 = 0.9956$ and 0.9549 for adsorption of Pb(II) and ARS respectively gave good fit to the adsorption processes. The ΔG° obtained were negative which is an indication of spontaneous adsorption processes, while the positive values of ΔH (+143.46 and +84.50 KJ/mol) and ΔS (+0.473 and +0.364 KJ/mol) for Pb(II) and ARS respectively, revealed endothermic and randomness at the ZnO-aqueous interface during the adsorption processes. The E_a were found to be +6.193 and +6.956 KJ/mol for adsorption of Pb(II) and ARS respectively which showed that the adsorption onto ZNPs is a physical process.

Keywords: ZNPs-adsorbent; synthesis/characterization; adsorption; isotherms; kinetics; thermodynamic

1.0 Introduction

Rapid industrial growth paralleling the swift rise in civilization and modernization resulting in industrialization is raising a global concern by generating huge volumes of toxic materials into the environment especially water pollution. Amongst the various water pollutants, heavy metal ions and dyes require special attention because of their toxic nature and effects on humans and the environment. Most of the industries discharge wastewater and their effluents containing toxic materials into rivers without adequate treatment [1]. The amount of contaminated water is drastically increasing as a result of world population growth, global warming and industrial revolution [2]. Removal of contaminants and recycling of the purified water would provide significant reductions in cost, time and energy to the industry and result in improved environmental management and stewardship. Innovative use of nanoparticles for treatment of industrial wastewater is a potentially useful application for solving environmental challenges. Synthesis and application of inorganic nanoparticle as adsorbents for treating wastewater and industrial effluents have received a wide attention recently [3]. A number of physical and chemical properties make nanomaterials particularly useful for wastewater purification [4]. Recent researches had indicated that use of nanomaterials as adsorbents is a very useful and powerful tool for the removal of metal such as; Ni^{2+}, Cr^{6+}, Cu^{2+}, Cd^{2+}, Co^{2+}, Hg^{2+}, Pb^{2+}, As^{3+}, As^{5+}, Th^{4+}, Eu^{3+}, Sr^{2+}, Zn^{2+} and U^{6+} due to their unique structure and specific surface characteristics. Nanomaterials formed by metal or metal oxides are the inorganic nanoparticles, which are broadly used for the removal of the hazardous metal ions. Metal oxides possess minimal environmental impact, low solubility and even do not lead to any secondary pollution; they have also been widely adopted as adsorbents in many researches [4]. These unique and specific properties of nano-sorbents made them ideal materials for wastewater treatment technology because of their rapid adsorption of pollutants from aqueous phases or mediums. Most of the methods such ion exchange, electrolysis, reverse osmosis, coagulation and so on, used for removal of pollutants from wastewater have several disadvantages such as chemical requirements, time consuming procedure, production of large amount of sludge, low efficiency and high cost. However, adsorption method is considered to be more efficient, cost effective and free from

sludge formation [5]. Adsorption by nanoparticle adsorbents is effective in solving environmental problem owing to their large surface areas. For example, in an adsorption experiment, Pectin-Iron oxide magnetic nanocomposite was effective in removal of copper [6]. Piao *et al*. 2012 [7], adsorption work of Pb ions on nanoparticles of Iron oxide composite revealed that adsorbent was efficient over 5 cycles at about 90 %. Similarly, Andal, 2014 [8] investigated magnetic Fe_3O_4 adsorption of some metals ions from multi-component system and reported its adsorption capacity was well over 90 %. Nanohybrid graphene oxide and Azide modified Fe_3O_4 nanoparticles were fabricated using Click reaction and used for adsorption of some dyes and the adsorption capacities were high [9]. Similarly, the adsorption of Crystal Violet from synthetic wastewater on ferrite nanocomposite was above 90 %. The report of the work concluded that removal efficiency might be increased by using more adsorbent weights in proportional volume of various concentrations [10]. The work of Zeinab and Mohammed 2015 [11], on TiO_2 nanoparticles showed about 65 % removal of Malachite Green dye in the dark, while irradiation of the dye increased the removal percentage to 80 %. Nevertheless, fewer adsorbents have performed satisfactorily in the removal of pollutants from wastewater. This necessitated the search for a special method of growing crystal of ZnO oxide for effective removal of water pollutants from aqueous phases since it can with high thermal treatment and is easily available. Metal oxides such as ZnO can be synthesized and designed in different forms, such as particles, spheres, tubes, rods etc [4] and several studies have shown that nanoparticle especially metal oxide nanoparticles are effective and efficient adsorbents in the cleanup of environment as a result of their inherent ability to penetrate into area where pollutants are present [5]. Nanostructures of ZnO materials have received broad attention due to their distinguished performances in electronics, optics, and photonics [12] and are hydrophobic inorganic compound existing in white powder form. Their crystalline structures are hexagonal wurtzite, cubic zincblende and cubic rock salt with the wurtzite been the most stable of the three structures. Methods in conducting the synthesis of ZnO nanoparticles include direct precipitation, gas condensation, sol-gel synthesis amongst others [13].

This study was aimed at a special method of growing crystals of ZnO nanoparticles (ZNPs) for remediation of wastewater by adsorption on the synthesized nanoparticle adsorbent. The objectives of the study were to synthesize ZNPs adsorbent, characterize the prepared nanoparticles, and optimise the dependence of adsorption

of Cd(II) ions, and Alizarin Red S (ARS) from their aqueous solutions of wastewater at different conditions.

2.0 Experimental

2.1 Chemicals

Analyical grade chemicals were used throughout the experiment in this research work. The $Zn(NO_3)_2.6H_2O$ (hydrated zinc nitrate, 96.0 %) was supplied by MERCK, while NaOH (sodium, 97.0 %), KOH (potassium hydroxide, 85.0 %) and HCl (hydrochloric acid, 96.0 %) were obtained from FINAR. NICE supplied the CON_2H_4 (urea, 99.0 %), while Fisher scientific supplied the $PbNO_3$ $Pb(NO_3)_2$. (lead nitrate, 96.0 %) used in this adsorption work.

2.2 Synthesis of Nanoparticles (NPs) ZnO Adsorbent

The ZNPs were synthesized by adding 100 mL of 0.5 M solution of urea (CON_2H_4) to 100 mL of 0.1 M Zinc nitrate hexahydrate [$Zn(NO_3)_2.6H_2O$] salt solution with continuous stirring to 90 ^oC. The urea solution was gradually added to the stirring clear nitrate solution in drops until it was exhausted within the first hour. The supernatant was left for extra 2 hr after complete addition of urea solution to allow for nucleation and growth of ZNPs. The resultant solution was cooled, washed several times with a mixed solution of ethanol, and distilled water to release soluble ions such as NO_3^{2-} and was filtered using whatman no. 42 filter paper. The nanoparticles sample obtained was transferred to a crucible fitted with a cap and heated for 3 hr at 500 ^oC in a furnace. The ZNPs prepared was taken for characterization and further use. According to Husari et al. 2013 [14] and Godwin *et al.* 2022 [15], the progressions of the crystal growth and nucleation of ZNPs in the presence of urea are represented in steps 1 to 5 (Eqs. 1-5);

Step I: urea was dissolved in water to produce ammonia according to Eq. 1;

$$CO(NH_2)_2\,(s) + 3H_2O(l) \rightarrow CO_2(g) + 2NH_3(g) + 2H_2O(l) \quad (1)$$

Step II: ammonia generated ammonium ions which increased the pH aqueous solution that supported the growth of ZNPs crystal as temperature was increased according to Eq. 2;

$$CO_2(g) + 2NH_3(g) + 2H_2O(l) + e^- \rightarrow OH^-(aq) + HCO_3^{2-}(aq) + 2NH_4^+(aq) \quad (2)$$

Step III: Zinc nitrate was dissolved in in water to produce Zn^{2+} ions according to Eq. 3;

$$Zn(NO_3)_2(s) + H_2O(l) \rightarrow Zn^{2+}(aq) + 2NO_3^-(aq) + \ H_2O(l) \quad (3)$$

Step IV: aqueous solution from step II and III were reacted to produce the hydrated zinc specie with high amount of the hydroxide ions in Eq. 4;

$$CO_3^{2-}(aq) + 4Zn^{2+}(aq) + 6OH^-(aq) + H_2O(l) \rightarrow Zn_4CO_3(OH)_6(s) + H_2O(l) + 5e^- \quad (4)$$

Step V: the hydrated zinc specie decomposed on heating to produce ZNPs according to Eq. 5

$$Zn_4CO_3(OH)_6.H_2O(s) \rightarrow 4ZnO(s) + 4H_2O(s) + CO_2(g) \quad (5)$$

2.3 Characterization

The Emperean series 2 was utilized in the analysis of XRD spectra of ZNPs, while the PAN-analytical (BBHD10-90.xrdmp) measurement software was used to record the XRD pattern. A CuKα (1.54060 Å) at 40 kV and 45 Ma at a scan step of 24.765 sec. (25 ºC) was used for the XRD analysis in the 2Θ = 20 to 90º interval. The Zeiss Evolution model SEM equipped with $LaBr_6$ filament was used to determine the morphology of the prepared NH sample by gold coating 10 mg of the nanomaterials with a carbon film for 15 min at 40 μA at a scan speed 7. The coated material was introduced into the sample holder for SEM analysis and a 4.14 mbar vacuum was created to reach -0.05 mbar before the SEM experiment was started. The Tecnai G2 20 twin was used for the TEM analysis of the NH sample. A 10 mg of the nanomaterial sample was dispersed in a beaker containing 5 mL of ethanol and was ultrasonically shaken for 15 min. At the completion of uniform dispersion, 0.5 μL of the supernatant was smeared on a carbon film and allowed to dry with the aid of an infrared source of light for 2 min. A single tilt sample holder was used to load the dried sample and the loaded carbon film was inserted into the TEM vacuum pipe for analysis. The NICOLET 6700 digital spectrometer with a Kbr detector pellet was used for the FTIR experiment, and the spectra data was recorded from 4000 cm^{-1} to 500 cm^{-1}. The Anaton paar LENOVO leitesizer 500 was used to determine the particle size distribution of the synthesized ZNPs. The Dynamic Light Scattering (DLS) was used to determine the average particle size distribution of ZNPs. The DLS spectrometer was equipped with a 660 nm laser and at 25˚C for particles sizing experiment. The surface area of the ZNPs was carried out using the data obtained by Brunauer-Emmette-Teller (BET) method of calculation. The Nitrogen (N_2) physisorption experiment was performed by taking 2 mg of the dried ZNPs sample and heated under vacuum for 10 hr at 100 ºC after dispersion of the samples on a quantrachrone cell experiment. The effect of mass loss as a result of temperature change was performed with a TGA/DTG Setaram evolution instrument at a heating rate of 10 ºC min^{-1} in an inert N_2 atmosphere. The mass loss steps, degradation process and thermal stability of ZNPs was determined by TGA-DTA.

2.3.1 Determination of ZnO NPs Point of Zero Charge (pH_{pzc})

The point of zero charge (pzc) of ZNPs adsorbent was performed using the salt addition method with potassium nitrate solution (0.1 M). The salt solutions were prepared in the range of 2.0 to 12.0 in various conical flask and a 0.1 g mass of the ZNPs was measured and dispersed in each of the 50 mL solutions in the conical flask. The resultant mixture was agitated in an orbital sharker (smitta scientific as 30) at 120 rpm for 2 hr. The initial pH ($pH_{initial}$) and final pH (pH_{final}) of each of the salt solutions containing the NPs sample were recorded and plotted against each other from where the curve for pH_{pzc} of the ZNPs was estimated.

2.5 Batch adsorption studies

Different initial concentrations of Pb ions (100 to 900 mg/L) and ARS (5 to 60 mg/l) were used to determine the equilibrium concentration for optimizing the adsorption capacity of ZNPs adsorbent at various conditions. The metal ions adsorption experiments were performed initially by contacting 50 mL of the metal ions and dye solution in a conical flask with 1 mg of the ZNPs adsorbent at 34 ^{o}C (prevailing room temperature). The adsorbent-adsorbate solutions in the conical flasks were agitated in the magnetic orbital shaker at 120 rpm and separated by filtration through Whatman no.42 filter paper, and the filtrate was immediately analyzed using ICP-OES (thermo-scientific iCAP 700 series) and UV-Spectrophotometer (Perkin Elmer Lambda 35) for Pb ions and ARS concentrations at equilibrium respectively. The equilibrium concentrations (C_e) after adsorption were determined and recorded for each set of the experiments. The effect of factors such as of agitation time (5, 10, 20, 30, 60, 90, 120, 150, 180 and 240 min), adsorbent dose (0.05, 0.10, 0.15, 0.20 and 0.25 g), pH (2, 4, 6, 8 and 10) of solution, and temperature (293, 298, 303, 308, 313 and 318 K) were studied by equilibrating with 50 $cm^{-3}$of each metal ions and dye solution in a conical flask and shaken for 2 hr at 120 rpm. In each case, the C_e were determined for each set of the adsorption experiments. The pH of the solutions were adjusted with 0.1 M of HCl and/or NaOH were necessary. The adsorption capacities (q_e) and the removal efficiency (% R) were determined using Eqs. 6 and 7 respectively, where the C_o is the initial concentration, and the m and V were the mass (g) of adsorbent, and volume (L) of solution (mg/L) respectively. The kinetics models (pseudo-first order, pseudo-second order, and intra-particle diffusion), isotherm models (Langmuir, Freundlich and Tempkin) and thermodynamics were used to test the adsorption data.

$$q_e = \frac{C_0 - C_e}{m} X\ V \tag{6}$$

$$\%\ R = \frac{C_0 - C_e}{C_0} X\ 100 \tag{7}$$

2.6 Isotherm studies

The isotherm studies is predicted by empirical relationships that determines the amount of sorbate (Pb ions and ARS) molecules absorbed by a solid sorbent in the adsorption process. By graphical representation of the quantity adsorbed (q_e) by a unit mass of the adsorbent, and the amount of adsorbate left in solution at the equilibrium (C_e), the adsorption data can be obtained and isotherm parameters estimated [15, 16]. The Langmuir, Freundlich, Temkin and Dubinin-Raduchkevich adsorption isotherms were applied to this batch adsorption experiment using the least square fit method.

The Langmuir adsorption isotherm assumes homogeneous and monolayer adsorption, [17] and includes a Langmuir adsorption constant that indicates maximum quantity (q_m) adsorbed at equilibrium [16]. The Eq. 8 is a linear form of the Langmuir isotherm;

$$\frac{C_e}{q_e} = \frac{1}{q_m K_L} + (\frac{1}{q_m})C_e \quad (8)$$

where; q_m (mg/g) is the maximum adsorption capacity of the NPs adsorbent, while K_L (L/mg) is the equilibrium constant. The q_m and K_L were determined from the plot of Ce/q_e verses C_e where the factor $1/q_m K_L$ and $1/q_m$ were estimated from the intercept and slope respectively. The R_L factor (determinant of nature of adsorption) was estimated from Eq. 9;

$$R_L = \frac{1}{1+ K_L} \quad (9)$$

where; R_L = 1 (linear adsorption), R_L< 1 (favourable adsorption), R_L > 1 (unfavourable adsorption) and R_L = 0 (irreversible adsorption).

The Freundlich adsorption isotherm model is used to describe a multilayer and heterogeneous adsorption [16]. The linear isotherm equation which describes Freundlich adsorption are represented in Eqs. 10 and 11 respectively;

$$q_e = K_f C_e^{1/n} \quad (10)$$

$$\log q_e = \log K_f + \frac{1}{n}\log C_e \quad (11)$$

where; K_f and n are the Freundlich constants related to adsorption capacity (mg/g) and heterogeneity of the adsorbent surface respectively. The constants were obtained from the plot of $\log q_e$ verse $\log C_e$ where the factors $logK_f$ and $1/n$ were equated with the intercept and slop of the linear equation respectively.
The Temkin isotherm equation is represented in Eq. 12, while its B_T factor was estimated from Eq. 13;

$$q_e = \frac{RTInA}{b_T} + \frac{RTInC_e}{b_T} \quad (12)$$

$$\frac{RT}{b_T} = B_T \quad (13)$$

where; R is the universal gas constant with the value 8.314 J/mol, b_T is Temkin constant, A is the isotherm binding constant (L/g), and T is Kelvin temperature Kelvin. The Temkin constants was estimated from the plot of q_e verses InC_e, where the factors B_TInA and B_TInCe were estimated from the intercept and slope of the equation respectively, and B_T was obtained from Eq. 13.
Dubinin, Polanyi, and Radushkevich (D-R) is a simple but very useful empirical theory allowing one to estimate the quantity of solute adsorbed at equilibrium [18]. The theory was based on a pore filling model. It assumes a multilayer adsorption behaviour involving Van Der Waal's forces and is applicable to physical adsorption processes [19].The linear form of the D-R isotherm equation is given in equation14.

$$lnq_e = Inq_m - K_{DR}\varepsilon^2 \quad (14)$$

The Ɛ parameter is calculated thus;

$$\varepsilon = RTIn\left(1 + \frac{1}{Ce}\right) \quad (15)$$

$$E_{D-R} = \frac{1}{\sqrt{-2K_{D-R}}} \quad (16)$$

where: $K_{D\text{-}R}$ is a constant ($mmol^2/J^2$) which related to the activity coefficient constant which gives the free energy, $E_{D\text{-}R}$ (Eq. 16), Ɛ is Polanyi potential ($Jmol^{-1)}$, R is universal gas constant (8.314 J/molK) and T is temperature (K). The factor Inqe was

estimated from the plot of Inq_m *vs* Ɛ.

2.7 Kinetic studies

The adsorption of the metal ions and dye onto the ZNPs adsorbent were studied using pseudo-first order, pseudo-second order and the intraparticle diffusion models. The pseudo-first order and pseudo-second order are represented in Eqs. 17 and 18 respectively;

$$In(q_e - q_t) = Inq_e - K_1 t \quad (17)$$

$$\frac{t}{q_t} = \frac{1}{K_2 q_e^2} + \frac{1}{q_e} \quad (18)$$

where; q_t is the amount (mg/g) adsorbed on the adsorbent at time, t, and K_1 and K_2 are the rate constants for the pseudo-first order and pseudo-second order adsorption kinetics respectively. The constants q_e and K_1 were estimated from the plot of $In(q_e - q_t)$ verse t in the first-order equation while the plot of t/q_t verses t was used to determine constants q_e and K_2 for the second-order.

Intraparticle diffusion model describes surface diffusion and the equation is represented in Eq. 19;

$$q_t = K_i t^{0.5} + I \quad (19)$$

where; K_i is a diffusion constant in mg/g, and I is related to the boundary layer thickness in mg/gmin$^{0.5}$. The linear plot of q_t verses $t^{0.5}$ were used to determine the constants K_i and I which were the slope and intercept respectively. The larger values of I indicate thickability of the adsorbent surface which results in slow rate of adsorption, while larger values of K_i describes better adsorption.

2.8 Thermodynamic studies

The thermodynamics of adsorption are better understood by determining the ΔH (enthalpy change), ΔG (free energy change), ΔS entropy change (entropy change) and E_a (activation energy) of adsorption. The ΔH and ΔS positive values describe endothermic and random adsorption, while of ΔG negative values indicate spontaneous adsorption [16]. Generally, for physical adsorption, the ΔG values are in the range of -20 to 0 kJmol^{-1}, while chemical adsorption are in the range of 80 to 400 kJmol^{-1} [20]. For physical adsorption, ΔH has values between 2.10 to 20.90 kJmol^{-1}, while 80 to 200 kJmol^{-1} describes chemical adsorption. The values of E_a < 40 kJmol^{-1} indicates physical adsorption (controlled by diffusion) while larger values

indicate chemical adsorption [21, 16]. The ΔH and ΔS were estimated from Eq. 20, while ΔG and E_a were determined from Eqs. 22 and 23 respectively;

$$InK_{ad} = \frac{\Delta S}{R} - \frac{\Delta H}{RT} \quad (20)$$

$$K_{ad} = \frac{q_e}{C_e} \quad (21)$$

$$\Delta G = -RTInK_{ad} \quad (22)$$

$$Ink_2 = InA - \frac{E_a}{RT} \quad (23)$$

where; K_{ad} is the distribution coefficient which was estimated from Eq. 21, R is universal gas constant, k_2 is the second-order rate constant, and A is the Arrhenius constant which is represent the fraction of the adsorbate with the right orientation to be adsorbed onto the adsorbent. The ΔH values were estimated from the slope and intercept resulting from the linear plot of InK_{ad} verses *1/T,* while the plot of Ink_2 verses *1/T* was used to calculate A and E_a from the slope and intercept respectively. The isotherm parameters in this adsorption studies were estimated by minimizing error function using Microsoft Excel Solver.

The RMSE (Root Mean Square of Errors) function as expressed in Eq. 24 was used in this work to measure the goodness of fit between the experimental data obtained and the theoretical models;

$$RMSE = \sqrt{\frac{\sum_{i=0}^{n} (q_{e,exp} - q_{e,cal.})^2}{N}} \quad (24)$$

where the $q_{e,exp}$ and $q_{e,cal}$ indicate the experimental and calculated amount adsorbed and *N* is the number of measurement taken from the adsorption experiment. Lower RMSE value is an indication of a better fitting curve of the isotherm models that describe the system.

3.0 RESULT AND DISCUSSION

3.1 Characterization

The XRD pattern was indexed to the crystalline hexagonal phase of the ZNPs with lattice constants of a = 3.264 Å and b = 5.219 Å as observed in Fig. 1a. The characteristic peaks observed for the synthesized ZNPs agreed with those taken from the Joint Committee of Powder Diffraction Standards (JCPDS) card No.36-1451. The results obtained from the XRD spectrum of the synthesized ZNPs indicated sharp and narrow peaks, confirming that the sample is of high quality with good crystallinity and fine grain sizes. The definite line broadening of the diffraction peaks for ZNPs also explains that the prepared ZNPs were in nano- range and no characteristics peaks were observed other than ZnO. The XRD pattern showed lines at 2θ values equal to 31.81, 34.31, 36.23, 47.62, 56.71, 62.92, 66.32, 67.00, 69.13, 72.63, and 76.92 corresponding to (100), (002), (101), (102), (110), (103), (200), (112), (201), and (202), with the strongest peak lines at 31.81, 34.31, and 36.23 as a result of reflection from the crystallographic (100), (002) and (101) planes [16, 22]. The Debye-Scherer formula was used to calculate the average crystal size of the synthesized ZNPs according to Eq. 25:

$$K = \frac{0.9\lambda}{\beta cos\Theta} \tag{25}$$

where, the particle shape factor was taken to be 0.9, λ is the wavelength of the CuKα radiation, and β the Full Width at Half Maximum (FWHM) of the diffraction peak in radian which corresponds to the Bragg diffraction angle (2θ). The crystal size of ZNPs estimated by Eq. 25 was 35.69 nm which confirms the size of the nanomaterial. The FTIR analysis of ZNPs is shown in Fig. 1b. The most important peak positions were found at 3452.6, 1635.4, and 420.29 cm^{-1}. The peak at 3452.6 cm^{-1} is due to O-H stretching in surface water molecule, while the peak at 1635.4 cm^{-1} corresponds to bending vibration of H-O-H as a result of adsorption of moisture by the sample [16, 23, 24]. The band at 420.29 cm^{-1} is attributed to the stretching vibration of Zn-O. SEM images of the prepared ZNPs at different magnifications are presented in Fig. 2. The synthesized ZNPs are spherical in structures comprising of thin layers with uniform shapes and sizes. The ZNPs prepared also possessed porous structures on the crude surface. The EDAX of the selected areas in Fig. 2c showed that ZNPs contained zinc and oxygen. The aggregation of the ZNPs may be due to

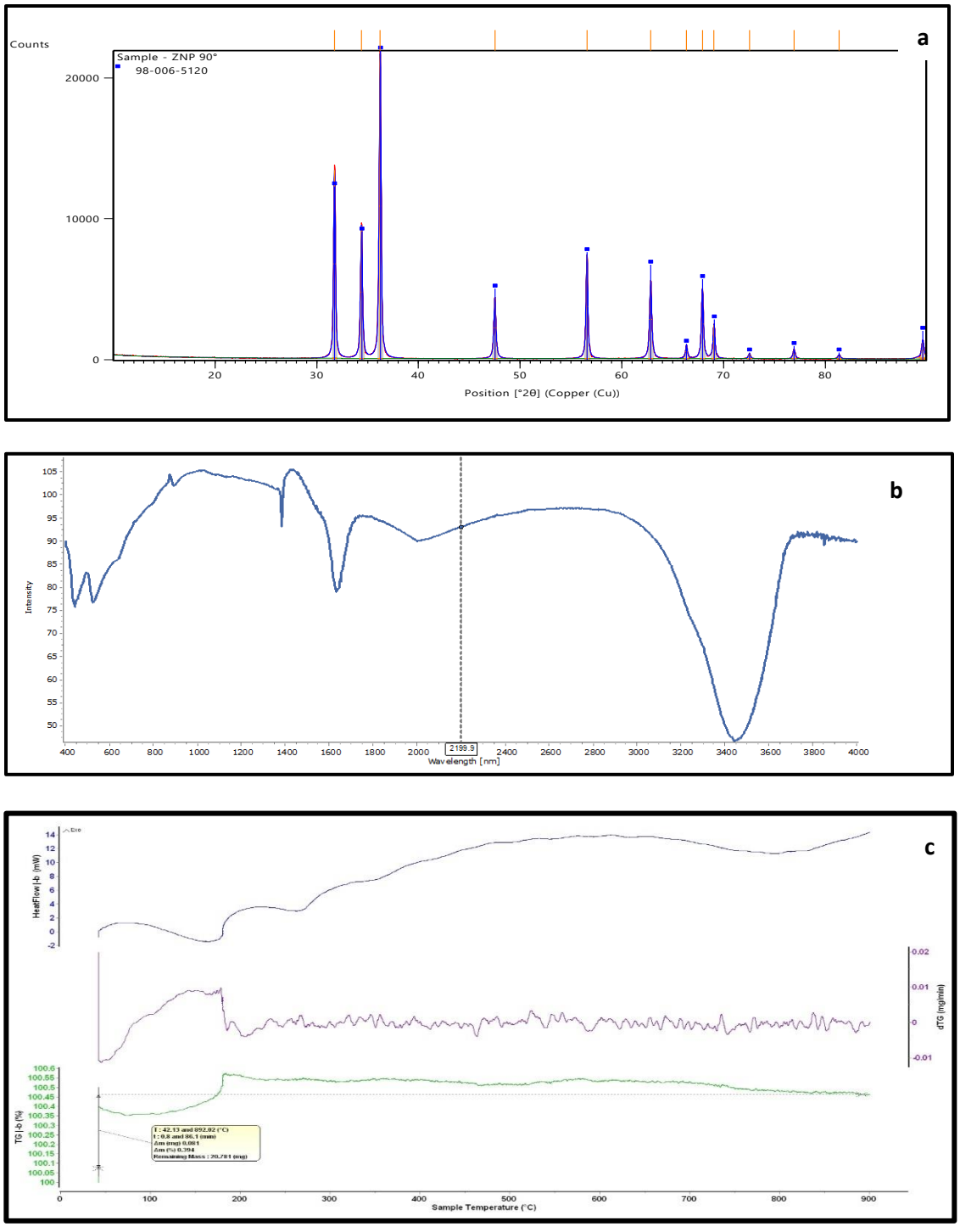

Fig. 1: XRD (a), FTIR (b), (c) and TGA/DTA (e) of ZNPs.

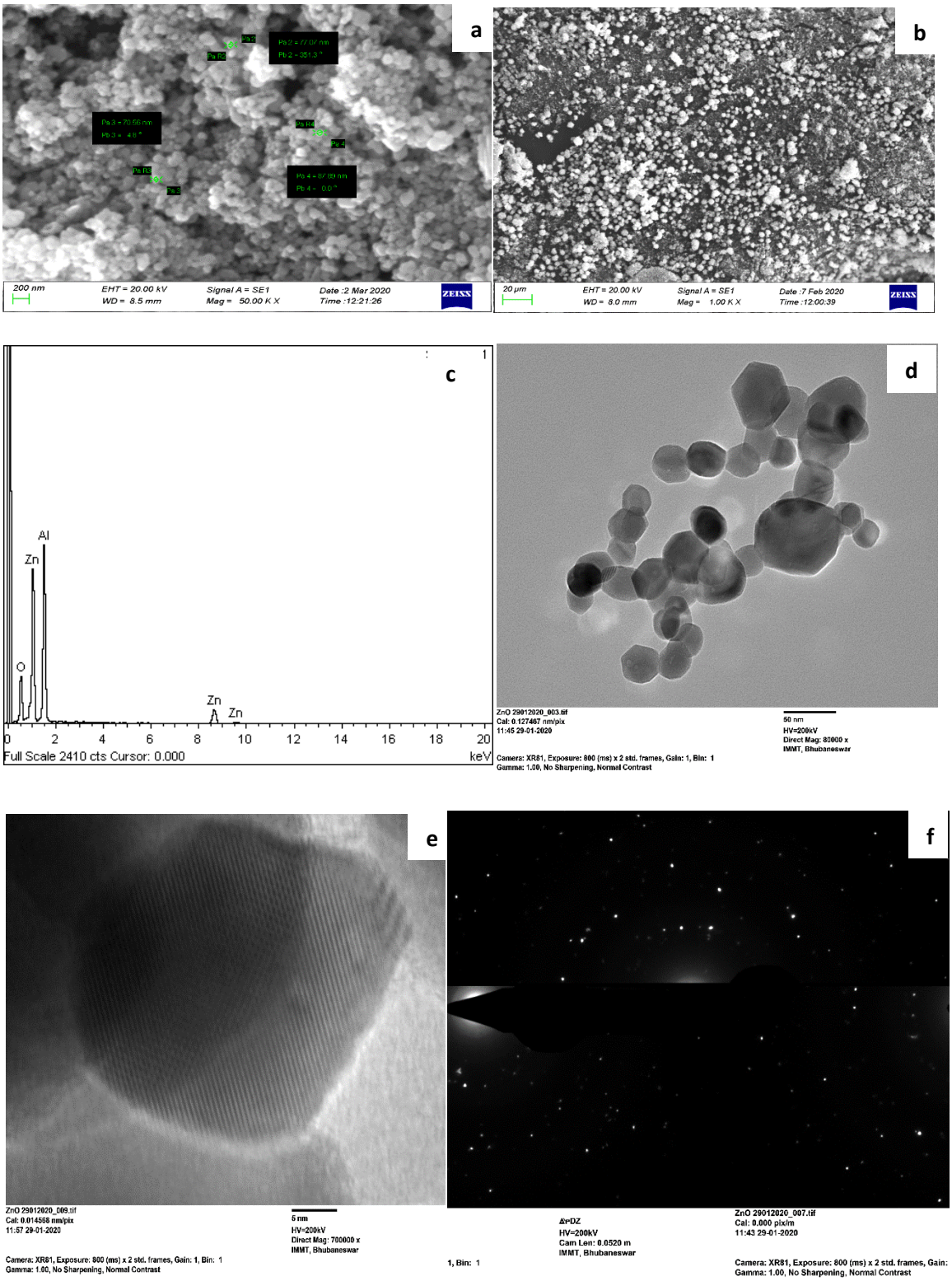

Fig. 2: SEM images (a - b), EDAX spectra (c) and TEM patterns; lattice fringes (d), lattice planes (e), and SAED image (f) of ZNPs-adsorbent.

high energy surface particles [25]. The DLS results of ZNPs for particles sizing revealed that synthesized material has an average particle sizes of 52.76 nm. The final pH (pH_{final}) of the solution was measured and the pH_{pzc} was determined by plotting the graph of the difference in pH_i and pH_f (ΔpH). The pH_{pzc} of ZNPs-adsorbent was found to be 6.53 [24, 26, 27]. The TEM images for the prepared ZNPs-adsorbent at different magnifications are presented in Fig. 2d - f. The lattice fringes (Fig. 2d), by observation, possessed hexagonal structures, the lattice plane (Fig. 2e) indicated that the ZNPs were in single phase, while the bright spots in the SAED image (Fig. 2f) showed that the ZNPs were crystalline and within the nano-range. This is in agreement with the XRD results. The TG/DTG curve indicated mass loss up to 171.9 °C for ZNPs as shown in Fig. 1c. The first mass loss steps for the ZNPs occurred between 0 °C to 105 °C, indicating the dehydration of water molecules adsorbed on the surface of samples. After this, the mass loss to 171.9 °C which may be due to loss of internally absorbed water molecules in the crystals structures of the nanoparticles. The second steps of mass loss may also be attributed to the decomposition and elimination of the volatile components that were still present on the synthesized nanomaterials surface after the synthesis. Anirudhan and Suchithra, 2010 [28] reported that removal of physiosorbed and interlayer water occurs between 90 to 200 ^oC while dehydroxilation (-OH group loss) takes place between 300 to 380 ^oC. The total weight loss under thermal decomposition of the ZNPs was 0.39 %. This indicated that the adsorbent was made up about 93.6 % of both ZNPs that were stable under the thermal condition. It also implied that the volatile components of the precursor material used to synthesize the nanomaterial were completely eliminated from the surface of the material. This observation of high thermal stability of ZNPs adsorbent under thermogravimetric analysis makes it a thermally stabled adsorbent under high thermal treatment during adsorption process. To identify the different mass loss steps, the TGA first derivative (rate of mass loss) was indicated in the TGA/DTA curve.

3.2 Effect of initial concentration and adsorbent dose on adsorption

The effect of initial concentration of the adsorption of Pb(II) and ARS onto ZNPs were carried out by agitating 0.10 g of the adsorbent with varying concentration of Pb(II) and ARS in a batch adsorption experiment. The result for the adsorption of Pb(II)ions and ARS onto ZNPs showed higher adsorption capacity with increasing concentration to an optimum point as represented in Fig. 3a and Fig 4a for Pb ions and ARS respectively. The adsorption capacity increases as the concentration

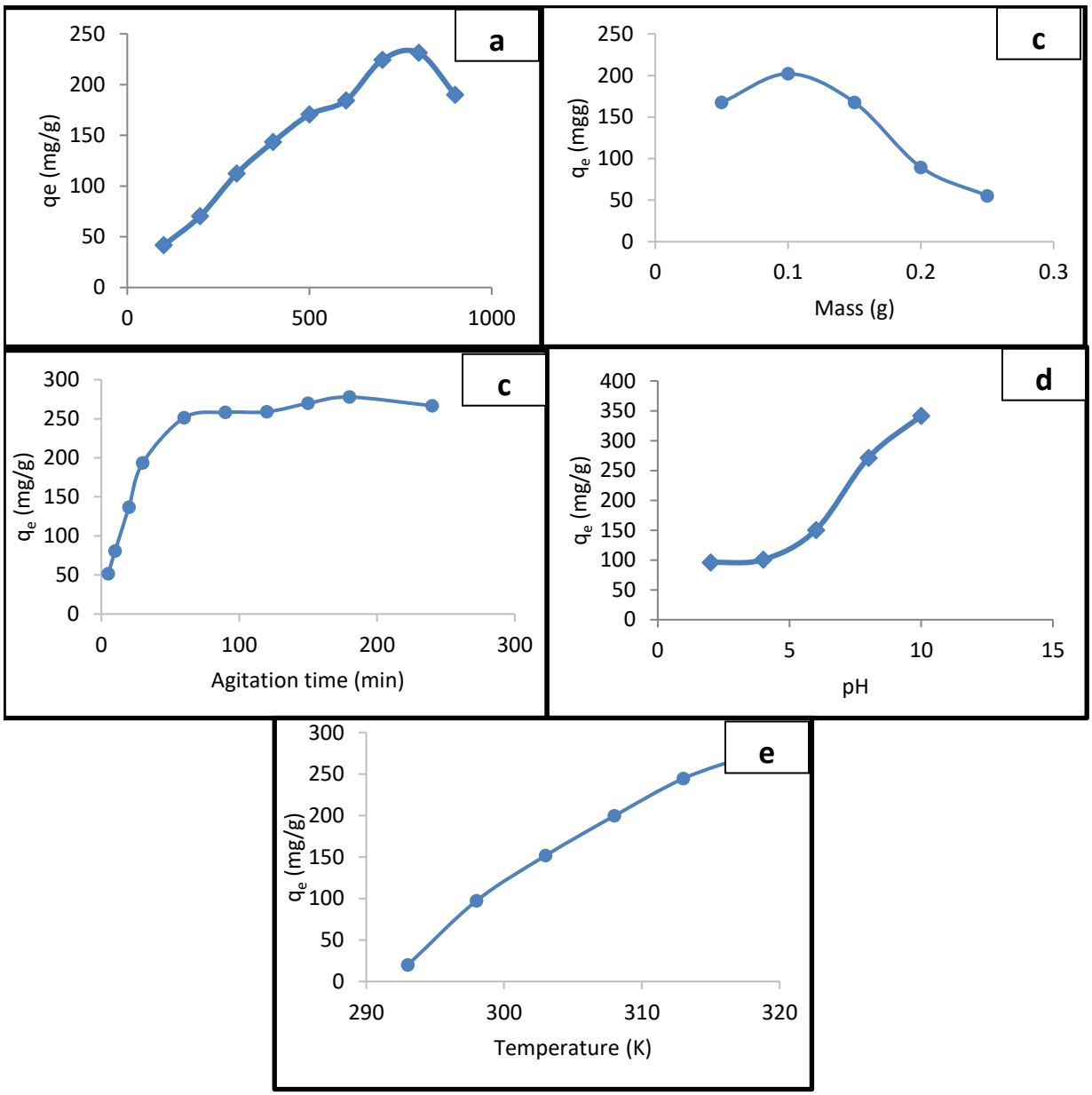

Fig. 3: Effect of initial concentration (a), adsorbent dose (b), agitation time (c), pH (d), and temperature on adsorption of Pb(II) onto ZNPs-adsorbent

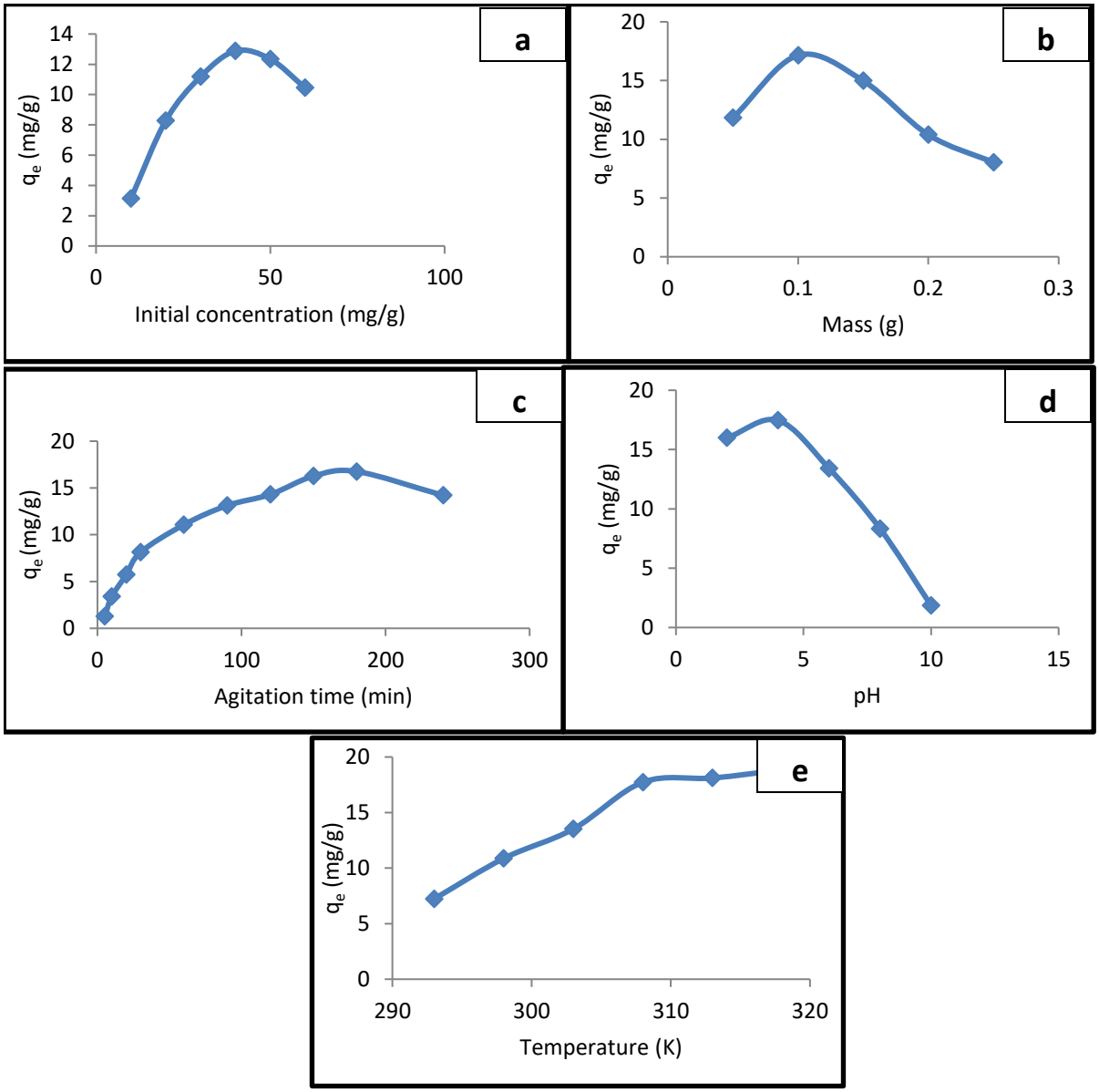

Fig. 4: Effect of initial concentration (a), adsorbent dose (b), agitation time (c), pH (d), and temperature on adsorption of ARS onto ZNPs-adsorbent

Table 1: Comparison of different adsorbents used for adsorption of Pb ions and ARS from aqueous phases

Adsorbent	Analyte	Quantity adsorbed (mg/g)	References
Activated char from neem	Pb(II)	205.6	[29]
Eucalyptus Camaldulensis	Pb(II)	9.259	[30]
GWTRs	Pb(II)	92.70	[31]
Silicate porous material	Pb(II)	44.83	[32]
Acid activated bentonite	Pb(II)	8.92	[33]
Fe_3O_4/rGO	Pb(II)	65.79	[34]
$NiFe_2O_4$	Pb(II)	168.0	[8]
Hydoxonium aluminum silicate mineral	Pb(II)	5.93	[35]
$MgCl_2$-loaded banana straw	Pb(II)	302.0	[36]
$MgCl_2$-loaded cassava straw	Pb(II)	200.06	[36]
ZNPs-adsorbent	**Pb^{2+}**	**341.65**	**This work**
CTAB modified alignate bound onto magnetite	ARS	16.89	[37]
Chitosane/ZnO	ARS.	8.01	[38]
n.Fe3O4- cover composite	ARS	10.74	[38]
Olive stone	ARS	10.90	[39]
ZNPs-adsorbent	**ARS**	**18.84**	**This work**

increases up to 800 mg/g and 50 mg/g for Pb(II) and ARS respectively, where equilibrium were established as shown in the figures for Pb(II) and ARS respectively. The efficiency of ZNPs in terms of optimum adsorption capacity was 18.84 and 341.65 for Pb(II) and ARS mg/g respectively. Comparison of these results with other works as represented in Table 1 reveals that ZNPs synthesized in this work has higher adsorption capacity for Pb ions and ARS. The decrease in performance of the adsorbent beyond the optimum level is due to the unavailability of adsorption sites as a result of adsorbent surface saturation. Lower initial concentrations of the adsorbate provided the driving force for the increase in adsorption rate to the optimum level where adsorption declined.

The effect of the adsorption of Pb(II) and ARSs onto ZNPs were performed by varying the mass of the adsorbent from 0.05 g to 0.25 g with a fixed concentration of Pb and ARS at 800 mg/g and 40 mg/l respectively in a batch adsorption mode. The adsorption capacity of ZNPs decreased with increase in mass of the adsorbent for adsorption of Pb(II) and ARS as represented in Fig. 3b and 4b respectively. The decrease in adsorption capacity of ZNPs as adsorbent dose increases may be due to

aggregation of the NPs as the mass increases. This is because the adsorption sites are shielded by the crowded ZNPs and the resultant effect is reduction in surface area of the adsorbent material. In this study, the optimum adsorption occurred when the mass dose was 0.10 g for both Pb(II) and ARS corresponding to 202.08 mg/g and 17.15 mg/g respectively. Comparison of this result with other reports as indicated in Table 1 shows that ZNPs is more efficient in the adsorption of Pb(II) and ARS.

3.3 Effect of agitation time and pH on adsorption

The effect of contact time on the adsorption of RB on the synthesized ZNPs is represented in Fig. 3c and 4c for Pb(II) and ARS respectively. An amount of 0.10g of the ZNPs was agitated with 50 mg/l of Pb(II) and ARS in a batch adsorption mode for a period of 5 to 240 min 30 ºC. Careful study of the results revealed that the adsorption capacity of the adsorbent increases with increasing agitation time to the optimum level beyond which further adsorption declined due to unavailability of active adsorption sites on the adsorbent. The adsorption rate was faster in the first 180 minutes with up to 277.75 and 16.75 mg/g adsorption capacity for Pb(II) ions and ARS respectively**.**

The pH plays an important role in the adsorption process because it is used to determine the mechanism of adsorption process. The effect of initial pH on the adsorption of Pb(II) ions and ARS onto ZNPs were performed by varying the pH from 2 - 10. The Fig. 3d and 4d show the effect of varying pH on the adsorption process. It can be clearly observed that there were a decrease in adsorption of Pb(II) and ARS onto ZNPs as the pH increases from 4 to 10. The optimum adsorption capacity for Pb(II) was reached at pH 10 ($pH_{pzc} > 8.53$) corresponding to 341.68 mg/g. The affinity of Pb(II) for the ZNPs beyond the point of zero charge is because the surface of the adsorbent becomes more negative resulting in interaction between Pb ions and the adsorbent surface. Similarly, The optimum adsorption capacity for ARS was reached at lower pH 4 ($pH_{pzc} < 8.53$) corresponding to 17.46 mg/g. Below the point of zero charge, the surface of the adsorbent becomes positive resulting in adsorption of ARS in acidic medium.

3.4 Effect of temperature on adsorption

The rate of diffusion increases as temperature increases leading to increased adsorption rate as a result of enhanced intraparticle diffusion. In this study, the effect of temperature on adsorption of Pb(II) and ARS onto ZNPs at different temperatures values was investigated and the results are shown in Fig. 3e and 4e. It was observed

that the rate of adsorption increases with increase in temperature. The optimum temperature for the adsorption of Pb(II) and ARS onto ZNPs were 318 K corresponding to 273.60 and 18.84 mg/g respectively.

Beyond 318 K, adsorption rate slopes drops which may be due to desorption as a result of increase in thermal energy which may result in the breakdown of the surface of the adsorbent material.

3.5 Isotherm Studies of adsorption

The Langmuir, Freundlich, and Temkin isotherm plots were used for the adsorption of Pb(II) and ARS on ZNPs. All the data represented fitted well to Langmuir isotherm with the regression coefficient, R^2, 0.9987 and 0.9035 of type 1 and type 2 Langmuir isotherms models for Pb(II) and ARS respectively, while Freundlich and Temkin were found to give low R^2 values as indicated in Table 2. The fitting of Langmuir adsorption isotherm model suggested that the adsorption of Pb(II) ions and ARS on ZNPs- adsorbent showed homogenous monolayer adsorption coverage. Further analysis of the Langmuir isotherm can be described on the basis of the separation factor, R_L which refers to a dimensionless equilibrium constant that indicates the sorbate-sorbent level of interaction [16]. The R_L values (Table 2) for the adsorption of Pb(II) ions and ARS on ZNPs were found to be lower than unity which is a description of favorability of the adsorption process ($0 < K_L < 1$).

This means that ZNPs is an excellent and efficient adsorbent for the adsorption of Pb(II) and ARS from aqueous solution.

Information about the mechanism of adsorption whether physisorption or chemisorption process can be obtained from E_{D-R} values. Its values between 8.0 to 16.0 kJ/mol correspond to chemical ion exchange while $E_{D-R} < 8.0$ kJ/mol indicates physical adsorption process [28]. The E_{D-R} values for adsorption of the Pb ions and ARS are presented in Table 2. It can be observed that the E_{D-R} values for the adsorption of Pb ions and ARS onto ZNPs were less than 8.0 kJ/mol which indicated physical adsorption. This result is in agreement with the Temkin isotherm studies above and can be concluded that the adsorption of the metal ion and dye onto all the ZNPs were physical mechanisms.

Table 2: Isotherm studies constants and regression coefficients for adsorption on ZNPs-adsorbent.

		Linearized equation	Plot	Isotherm parameters	Pb	ARS
Langmuir	Type 1	$\frac{C_e}{q_e} = \frac{1}{q_m K_{L1}} + (\frac{1}{q_m})C_e$	$\frac{C_e}{q_e}\ vs\ C_e$	q_m (mg/g)	243.9	12.35
				RL (L/mg)	0.9987	0.7596
				R^2	0.9987	0.9035
				K_L	0.0013	0.3164
				X^2	3.213	2.661
	Type 2	$\frac{1}{q_e} = \frac{1}{q_m} + (\frac{1}{K_{L2} q_m C_e})$	$\frac{1}{q_e} vs\ \frac{1}{C_e})$	q_m (mg/g)	122.32	6.73
				K_L	0.6651	2.5311
				R^2	0.7119	0.1119
				R_L	0.3223	0.9161
				X^2	12.21	4.78
	Type 3	$q_e = q_m - (\frac{q_e}{K_{L3} C_e})$	$q_e\ vs\ \frac{q_e}{C_e}$	q_m (mg/g)	199.36	21.23
				K_L	0.5556	0.2198
				R^2	0.7731	0.3211
				R_L	0.8222	0.5622
				X	7.99	10.89
	Type 4	$\frac{C_e}{q_e} = K q_m - K_{L4} q_e$	$\frac{C_e}{q_e} vs\ q_e$	q_m (mg/g)	299.55	2.88
				K_L	0.9112	0.7612
				R^2	0.4441	0.7112
				R_L	0.6889	0.4333
				X^2	42.22	9.55
Freundlich		$logq_e = logK_f + \frac{1}{n} logC_e$	$logq_e\ vs\ logC_e$	N	1.9231	2.9499
				K_F	10.00	1.8201
				R^2	0.8930	0.4054
Temkin		$q_e = \frac{RTInA}{b_T} + \frac{RTInC_e}{b_T}$	$q_e\ vs\ C_e$	b_T (Kj/mol)	43.69	1044.8
				BT (K^{-1})	58.33	2.431
				R^2	0.8560	0.4550
				K_T (L/mg)	0.1012	1.6340
D-R		$lnq_e = Inq_m - K_{DR}\mathcal{E}^2$	*Inqe vs* $\mathcal{E}$	K_{D-R} (mmol/J^2)	0.0008	0.0110
				q_m (mg/g)	15.39	5.2840
				E_{D-R} (J/mol)	5.00	6.757
				R^2	0.5198	08209

3.6 Kinetic studies of adsorption

The linearity of the plot with R^2 values of 0.9965 and 0.9549 for adsorption of Pb(II) ions and ARS respectively, revealed that the second-order kinetics best explains the adsorption process. As presented in Table 3, the second-order model plot gave q_e value that was very close to the experimental value compared to the value obtained for the first-order. The adsorption of Pb(II) ions and ARS onto ZNPs also followed intraparticle diffusion mechanism wit R^2 values of 0.8036 and 0.8798 for Pb(II) and ARS respectively. The model suggests three stages of adsorption which includes surface, internal and equilibrium diffusion which appear as contact time progresses [16]. Adsorption is quick in the first stage (surface diffusion) and then it gradually

slows in the second stage (internal diffusion) before stagnating and reaching a near-plateau (equilibrium diffusion) after approximately 180 min, as shown in Figs. 4c and 5c for Pb ions and ARS respectively. Generally, the rate of pollutants removal from aqueous phase is initially fast and gradually decreases as adsorption time increases until it reaches equilibrium. This process is due to large number of adsorption vacant sites that are available in the initial stage of adsorption. However, with time, the remaining vacant adsorption sites cannot be easily accessed due to repulsive forces between the solute molecules on the solid and bulk phases [16, 40].

Table 3: Kinetics Studies Constants and Regression Coefficients of adsorption onto ZNPs-adsorbent

Kinetics Studies parameters		Pb(II)	ARS
Pseudo-first-order	K_1 (min^{-1})	0.005	0.0110
	R^2	0.7900	6.36
Pseudo-second-order	K_2 (mg/g/min)	0.0004	0.0011
	R^2	0.9965	19.23
Intraparticle Diffusion	K_i ($mg/g/min^{1/2}$)	6.2090	0.7650
	I (mg/g)	196.9	0.8777
	R^2	0.803	0.0110

Table 4: Experimental and Calculated q_e for the adsorption onto ZNPs-adsorbent

Adsorbate	R^2		q_e(exp) (mg/g)		q_e(cal) (mg/g)
	First-order	Second-order	First-order	Second-order	
Pb(II)	0.7900	0.9965	79.80	277.8	285.7
ARS	0.5064	0.9930	5.06	16.63	14.18

3.7 Thermodynamic studies

The thermodynamic parameters for the adsorption of Pb(II) and ARS onto ZNPs have been reported in table 4. The positive values of ΔH and ΔS indicated that the

adsorption processes were endothermic and random at the ZNPs-aqueous interface, while the increase in negative values of ΔG as temperature increases showed the spontaneous adsorption process [41]. The values of ΔH for adsorption of Pb(II) and ARS were estimated to be +143.46 and +84.50 KJ/mol for Pb(II) and ARS respectively, which is an indication of a physical adsorption process (ΔH values between 2.10 to 20.90 KJ/mol) [34]. The values of ΔS for this adsorption studies were estimated to be +0.473 and +0.364 KJ/mol for Pb(II) and ARS respectively. This revealed randomness at the ZNPs-aqueous interface during adsorption processes. The values of ΔG obtained in this studies were between -20 to 0 KJ/mol which implied that the adsorption processes were also physical, while the activation energy (E_a) values were found to be +6.193 and +6.956 KJ/mol for adsorption of Pb(II) and ARS respectively (Ea < +40 KJ/mol) which shows that the adsorption onto ZNPs is a physical processes.

Table 5: Thermodynamics studies of the adsorption onto ZNPs-adsorbent

Analyte	Temp. K	ΔG (KJ/mol)	ΔH (KJ/mol)	ΔS(KJ/mol)	Ea (KJ/mol)	R^2
Pb^{2+}	293	+6.478	+143.46	+0.473	+6.193	0.966
	298	+1.603				
	303	-0.384				
	308	-1.123				
	313	-1.999				
	315	-2.464				
ARS	293	+1.388	+84.50	+0.364	6.956	0.9710
	298	-0.434				
	303	-1.853				
	308	-5.270				
	313	-5.878				
	315	-7.378				

4.0 Conclusion

Nanoparticles of Zinc oxide were prepared through by a special crystal growth and nucleation co-precipitation processes and was used for Pb(II) and ARS removal from aqueous phases. The adsorbent showed efficient performance owing to its high capacity to remove pollutants from the synthetic wastewater. The method was found to be dependent on pH, temperature and time. The adsorption of Pb(II) and ARS

onto the ZNPs achieved up to 341.65 and 18.84 mg/g respectively at equilibrium. This is significant when compared with the results of other works where metal oxides were used for adsorption of pollutants. The pseudo-second-order kinetics and intraparticle model were found to be applicable to the adsorption studies and the isotherm data fitted well to Langmuir model which is an indication that the adsorption process is monolayer and homogeneous at the adsorbent surface. The positive values of ΔH and ΔS indicated that the adsorption processes were endothermic and spontaneous at the ZNPs-aqueous interface during adsorption, while the increase in negative values of ΔG revealed that the processes were spontaneous. The E_a values also suggest that the adsorption of Pb(II) ions and ARS onto ZNPs is diffusion controlled (physical adsorption).

Competing Interests Statement

The authors declare that they have no known competing financial interests or personal relationships that could have appeared to influence the work reported in this paper.

Author Contributions

John Godwin and Abdus-Salam Nasir wrote the main manuscript, and data analysis, Prasanna Kumar Panda did the characterization, and Bankim Chandra Tripathy reviewed the manuscript.

Acknowledgments

Dr. John Godwin thanks the World Academy of Science (TWAS), and CSIR-Institute of Minerals and Materials Technology (CSIR-IMMT), India, for the Doctoral Fellowship award.

Thanks to the Director, Prof. S. Basu, and my host supervisor, Prof. Bankim Ch. Tripathy for the opportunity to carry out this research work in the CSIR-IMMT's hydro-electrometallurgy laboratory and for supervising the project.

References

1. S. Neeta, and S.K. Guptal. Adsorption of Heavy Metals; a Review. *International Journnal of Innovative Research in Science, Engineering and Technology,* 2016; 5 (2): 2267 – 2273.
2. B. Terrance. Application of Nanomaterials for the Removal of Hexachromium and their Biological Implication. *Research Journal Environmental and Earth Science,*

2016; 12 (6): 13 – 17.
3. B. Priya, S. Shubhra, D. Papita. and M. Aniruddha. Green Synthesis of Silver-Nanocomposite for Treatment of Textile Dye. *Nanoscience and Technology,* 2014; 1 (2): 1 - 6.
4. K.G.Vinod, I. Tyagi, H. Sadegh, S. Ram, A.H. Makhlout, and M. Bahnam. Nanoparticles as Adsorbent; a Positive Approach for Removal of Noxious Metal Ions: a Review. *Science, Technology and Development,* 2015; 34 (3): 195 - 214.
5. V. Manimozhi, N. Partha, E.K.T. Sivakumar, N. Jeeva, and V. Jaisankar. Preparation and Characterization of Ferrite Nanoparticles for the Treatment of Industrial Wastewater. *Digest of Nanomaterials and Biostructures,* 2016; 11 (3): 1017 - 1027.
6. J. Gong, X. Wang, G. Zeng, L. Chen, J. Deng, X. Zhang, Q. Niu. Copper (II) Removal by Pectin-Iron Oxide Magnetic Nanocomposite Adsorbent. *Chemical Enineering Journal*; 2012; 185 – 186: 100 – 107. DOI: 10.1016/j.cej.2012.01.050.
7. P. Xu, G. M. Zeng, D. L. Huang, C. L. Feng, S. Huc, M. H. Zhao, C. Lai, Z. Wei, C. Huang, G. Xin Xie, Z. F. Liu. Use of Iron oxide Nanomaterials in Wastewater Treatment: a Review. *Science of the Total Environment,* 2012; 424: 1 – 10.
8. V. G. B. Andal. Removal of Lead ions by $NiFe_2O_4$ Nanoparticles. *International Journal of Research in Engineering and Technology,* 2014; 3(1): 472 – 483.
9. M. Namvari, and H. Namazi. Clicking Graphene Oxide and Fe_3O_4 Nanoparticles Together: an Efficient Adsorbent to Remove Dyes from Aqueous Solutions. *International Journal of Environmental Science and Technology,* 2014; 11(6): 1527 – 1536.
10. R. Rahimi, K. Hamed, M. Rabbani, and R. Rahimi. Adsorption Removal of Crystal Violet (CV), a Carcinogenic Textile Dye, from Aqueous Solution by Conducting Polyaniline/Hollow Manganese Ferrite Nanocomposite. *Impact Polymer Journal,* 2010; 8(8): 8 – 10.
11. M.A. Zeinab, and A.A. Mohammed. TiO_2 Nanoparticles for the Removal Malachite Green from Wastewater. *Advance in Chemical Engineerinng and Science,* 2015; 3(5): 373 – 388.
12. N. Kamellia, R. Zolfaghar, and P. Pakizevand. Synthesis of ZnO Nanoparticles and Investigation of the Ionic Template Effort of their Size and Shape. *International Journal of Nanotechnology,* 2011; 1(2):75 - 81.
13. A. Hasampour, M. Niyaifar, and M. Asan. Synthesis and Charaterization of Fe_3O_4 and ZnO Nanocomposite by Sol-gel Method. *Proceeding of the 4th International Conference Nanostructures, Kish Island, I. R Iran,* 2012. pp 205.
14. F.S. Husari, S.M Ali, A. Abaziz, and M. Rusop. Special Effect of Urea as a Stabilizer in Thermal Immersion Method to Syntesize Porous Zinc Oxide Nanostructures. *Journal of Nanomaterials,* 2013; 11: 1 – 7.
15. J. Godwin, J.R. Njimou, N. Abdus-Salam, P.K. Panda, B.C. Tripath, M.K. Ghosh, S. Basu. Nano-scale adsorben carefully designed for Kinetic and thermodynamics

of Rhodamine B. Inorganic Chemistry Communications, 2022; doi.org/10.1016/j.inoche.2022.109287.
16. F. Mehradad, H. Seyydeh-Cobra, Y. Jac-kyu and S. Mehdi: Application of ZnO-Fe_3O_4 Nanocomposite to the Removal of Azo Dye from Aqueous solution: Kinetics and Equilibrium Studies. *Water, Air and Soil Pollutants,* 2014; 225:2113.
17. K. Nalwa, A. Thakur and N. Sharma: Synthesis of ZnO Nanoparticles and its Application in Adsorption: Advanced Materials and its Applications in Adsorption. *Advanced Materials Proceedings,* 2017; 2(11): 697 – 703.
18. S. T. Abbas. Isotherm, Kinetic and Thermodynamics of Adsorption of Heavy Metal ions onto Local Activated Carbon. *Aquatic Science and Technology,* 2012; 1(2): 57 – 61.
19. N. Ayawei, A.N. Ebelegi, and D. Wankasi. Modelling and Interpretation of Adsorption Isotherms. *Hindu Journal of Chemistry,* 2017: 2 – 13.
20. N. Abdus-Salam and M. Buhari: Adsorption of Alizarin and Fluorescein Dyes on Adsorbent Prepared from Mango Seed. *The pacific Journal of Science and Technology,* 2014; 15(1):232 – 244.
21. N. S., Rao and Rao, M. B. Structural and Optical Investigation of ZnO Nanoparticles Synthesized from Zinc Chloride and Zinc Nitrate. *American Journal of Material Science, 2015;* 5(3): 66 – 68.
22. L. Anyu, Hua D. Yanhong J. Chenghui Ye, Bige Yu, Xinlan Z., and Aiying Ma. Super-efficient removal of heavy metals from wastewater by Mg-loaded Biochars: Adsorption Characteristics and Removal Mechanisms. *Langmuir*, Just Accepted Manuscript, 2020. DOI: 10.1021/acs.langmuir.0c01454.
23. D.T.C. Nguyen, H.T.N. Le, T.T. Nguyen, T.T.T. Nguyen, L.G. Bach, T.D. Nguyen, T.V. Tran, Multifunctional ZnO nanoparticles bio-fabricated from Canna indica L. flowers for seed germination, adsorption, and photocatalytic degradation of organic dyes, J. Hazard. Mater. 420 (2021) 126586. https://doi.org/10.1016/j.jhazmat.2021.126586.
24. N.A. Salahuddin, M. El-Kemary, E.M. Ibrahim, Synthesis and Characterization of ZnO Nanoparticles via Precipitation Method: Effect of Annealing Temperature on Particle Size, Nanosci. Nanotechnol. 5 (2015) 82–88.
25. S. Rahdar, A. Rahdar, M.N. Zafar, S.S. Shafqat, S. Ahmadi, Synthesis and characterization of MgO supported Fe–Co–Mn nanoparticles with exceptionally high adsorption capacity for Rhodamine B dye, J. Mater. Res. Technol. 8 (2019) 3800–3810. https://doi.org/10.1016/j.jmrt.2019.06.041.
26. J.R. Njimou, A. Măicăneanu, C. Indolean, C.P. Nanseu-Njiki, E. Ngameni, Removal of Cd (II) from synthetic wastewater by alginate -Ayous sawdust (*Triplochiton scleroxylon*) composite material, Env. Technol. 37 (2016) 1369–1381.
27. E. Kumar, A. Bhatnagar, W. Hogland, M. Marques, M. Sillanpää, Interaction of anionic pollutants with Al-based adsorbents in aqueous media – A review, Chem.

Eng. J. 241 (2014) 443–456. https://doi.org/10.1016/j.cej.2013.10.065.
28. T.S. Anirudhan, and P.S. Suchithra. Equilibrium, Kinetics and Thermodynamic Modelling for the Adsorption of Heavy Metals onto Chemically Modified Hydrotalcite. *Indian Journal of Chemical Technology,* 2010; 17: 247 – 259.
29. H. Patel. Batch and Continuous Fixed Bed Adsorption of Heavy Metals Removal using Activated Charcoal from Neem (*Azadirachtaindica*) Leaf Powder. *Scientific Report*; 2020; 10:16895. https://doi.org/10.1038/s41598-020-72583-6.
30. G. Hirut, G. Abraha, & D. Libargachew. Removal of Heavy Metals from Aqueous Solutions using *Eucalyptus Camaldulensis*: an Alternate Low Cost Adsorbent. *Cogent Chemistry*, 2020; 6:1, 1720892, DOI: 0.1080/23312009.2020.1720892.
31. W. Magdalena, K. Małgorzata, A. Kaufman, R. Grzegorz, and B. Tomasz. Removal of Heavy Metals and Metalloids from Water using Drinking Water Treatment Residuals as Adsorbents: a Review. *Minerals*; 2019; 9: 487. doi:10.3390/min9080487.
32. D. Ouyang, Y. Zhuo, L. Hu, Q. Zeng, Y. Hu and Z. He. Research on the Adsorption Behavior of Heavy Metal Ions by Porous Material Prepared with Silicate Tailings. *Minerals;* 2018; 9: 961.
33. P.P. Prathiksha, and P. Balakrishna. A Review on Removal of Heavy Metal Ions from Wastewater using Natural/ Modified Bentonite. *MATEC Web of Conferences* 144, 02021; https://doi.org/10.1051/matecconf/201814402021.
34. N. T. Hoan, N. T., Thu, H. V., Duc, N. D., Cuong, D, Q., Khiou and O., Vien: Fe_3O_4/Reduced Graphene Oxide Nanocomposite: Synthesis and Its Application for Toxic of Metal Ion Removal. *Journal of chemistry,* 2016; ID 2418172. Doi.10.1155/2016/2418172.
35. W. Enos, S.A. Paul, M. Shiundu and J. Wabomba. Removal of Heavy-Metals from Wastewater Using a Hydrous Alumino-Silicate Mineral from Kenya. *Chemical Society Ethiopia;* 2018; 32(1), 39-51.
36. A. Li, H. Deng, Y. Jiang, C. Ye, B. Yu, X. Zhou, and A. Ma. Super-Efficient Removal of Heavy Metals from Wastewater by Mgloadedbiochars: Adsorption Characteristics and Removal Mechanisms. *Langmuir*, Just Accepted Manuscript; 2020. DOI: 10.1021/acs.langmuir.0c01454.
37. K., Vijayalakshmi, Mahalakshmi, B., Latha, S., Gomathi, T., Sudha, P. N., Venkesan, J. and Anil, S. Batch Adsorption and Desorption Studies on the Removal Of Pb(II) from Aqueous Solution Using Nanochitosan/Sodium Alignate/Microcrystalline Cellulose Bead. *International Journal of Biological Macromolecules,* 2017 DOI:10.10116/j.ijbiomac.2017.04.120.
38. A. Omnia, and M. Sahar. Adsorption of Copper Ions and Alizarin Red S from Aqueous Solution onto Polymeric Nanaocomposite in Single and Binary Systems. *Turkish Journal of Chemistry,* 2017; 41: 967 – 986.
39. A.B. Albadarin, and C. Mangwandi. Chemistry Mechanism of Alizarin Red S and

Methylene B. Biosorption onto Olive Stone: Equilibrium and Kinetics. Paper Presented at the Third *International Conference on Water, Energy and Environment* (ICWEE), Shayah, UAE, 2015.

40. F. Najafi, O. Moradi, M. Rajabi, M. Asif, I. Tyagi, S. Agarwal, and V. K. Gupta. Thermodynamics of the adsorption of nickel ions from aqueous phase using graphene oxide and glycine functionalized graphene oxide. Journal of Molecular Liquids 208 (2015) 106–113. http://dx.doi.org/10.1016/j.molliq.2015.04.033.
41. J. Godwin, N. Abdus-Salam, H. I. Adegoke, P. K. Panda, J. Panda, and B. C. Tripathy (2022): Facile Synthesis of Rod-like α-FeOOH Nanoparticles adsorbent and its Mechanism of Sorption of Pb(II) and Indigo Carmine in Batc Operation. *Inorganic Chemistry Communications,* DOI: 10.1016/j.inoche.2022.109346.